

# FURTHER RESULTS ON ROBUST CONTROL OF MICROVIBRATIONS ON MASS LOADED PANELS

G. S. Aglietti<sup>\*</sup>, J. Stoustrup<sup>\*\*</sup>, E. Rogers<sup>\*</sup>, R. S. Langley<sup>\*\*\*\*</sup>, S. B. Gabriel<sup>\*</sup>,

<sup>\*</sup>Depts. of Aero & Astro/Electronics and Computer Science, University of Southampton, Southampton SO17 1BJ, UK etar@ecs.soton.ac.uk

<sup>\*\*</sup>Department of Control Engineering, Aalborg University, Denmark

<sup>\*\*</sup>Department of Engineering University of Cambridge, UK

## ABSTRACT

The suppression of microrvibrations (low amplitude vibrations with frequencies in the range 1 -1000 Hz) is now of critical importance in spacecraft and other applications and can only be achieved (in most cases) by active feedback control schemes. This paper uses a Lagrange Rayleigh Ritz method to develop a state space model of microvibrations arising in a vibrating panel with piezo-electric patches as actuators and sensors, disturbances and a payload. The resulting models are then used to design  $H_\infty$  based active feedback control schemes for disturbance attenuation.

## INTRODUCTION

Equipment onboard satellites is often mounted on lightweight panels where microvibrations have to be suppressed to achieve the required level of stability. In this work, attention is restricted to one such mass loaded panel which is an acceptable compromise between problem complexity and the need to gain useful insights as to the benefits (and limitations) of linear active control schemes. A schematic diagram of this so-called actively controlled panel (ACP) arrangement is shown in Figure 1 where the equipment mounted on the panel is modelled as lumped masses and the disturbances as point forces.

The sensors and actuators for the active control systems to be designed and implemented are twin patches of piezoelectric material bonded onto opposite faces of the panel. The bending vibrations of the plate produce a stretching and shrinking of the patches depending on whether they are on the top or on the bottom of the plate (Figure 2a). Due to the piezoelectric effect, these deformations induce an electric field perpendicular to the plate which is detected by the electrodes. The outer electrodes of

the patches are electrically connected together and the plate, which is grounded, is used as the other electrode for both patches of the pair (Figure 2a). The same configuration applies to the actuator, but here the electric field is applied externally to produce contraction or expansion of the patch, which will then produce a curvature of the plate.

Note that the effectiveness of the piezoelectric elements, both as sensors and actuators, decreases if the wavelength of the deformations is smaller than the patch. The essential reason for this reduced effectiveness is because the signal so produced is partially or completely (as in Figure 2b) cancelled by the opposing field generated by the other part of the patch as it is deformed in the opposite direction. This limiting factor is especially important when attempting to control high frequency vibrations which have, of course, very short wavelengths. One possible means of increasing the effectiveness of the patches in these situations would be to increase the patch dimension but care is needed since this would also diminish the control authority at low frequencies.

In the remainder of this paper, we outline the derivation of a state space model for the microvibrations induced on this panel and then proceed to use it to design  $H_\infty$  based active feedback control schemes for disturbance attenuation.

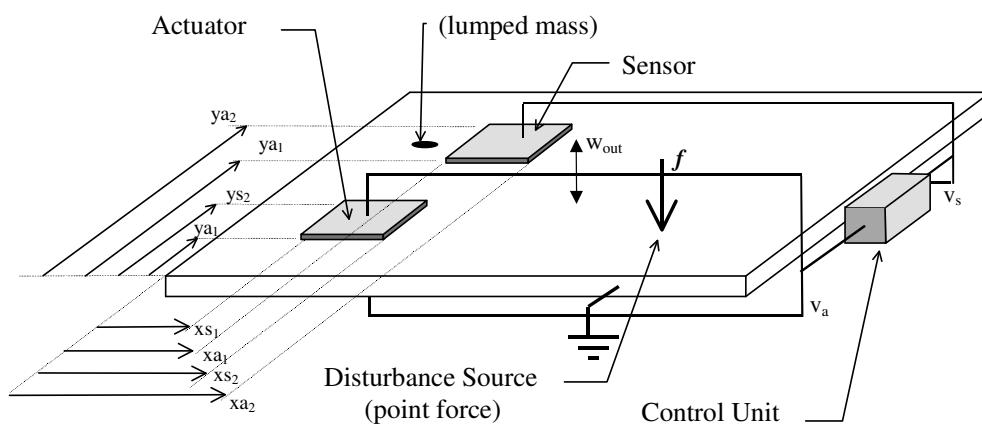


**Figure 1: Actively Controlled Mass Loaded Panel**

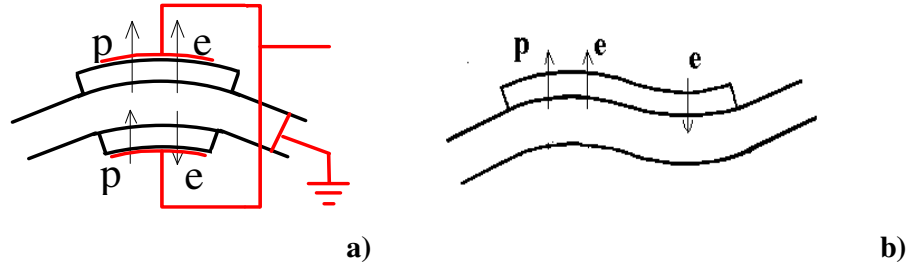


Figure 2: Cross section of the patch

### MATHEMATICAL MODEL

The mathematical model of the Actively Controlled Panel (ACP) is derived using the procedure described in detail in [1]. The first step of this procedure consists of writing suitable expressions for the kinetic and potential energy associated with the elements of the ACP, i.e. panel and piezoelectric patches.

The kinetic energies associated with the panel and the piezoelectric patches can easily be written as a function of the modal co-ordinates of the bare panel contained in the column vector  $\phi$ :

$$T_{pl} = \frac{1}{2} \dot{\phi}^t \mathbf{M}_{pl} \dot{\phi} \quad \text{and} \quad T_{pz} = \frac{1}{2} \dot{\phi}^t \mathbf{M}_{pz} \dot{\phi} \quad (1)$$

and similarly the potential energy associated with the panel can be written as:

$$U_{plate} = \frac{1}{2} \phi^t \mathbf{K}_{pl} \phi \quad (2)$$

In the case of piezoelectric patches, their potential energy can be expressed as the sum of three energy components

$$U_{pz} = U_{pz}^{elast} + U_{pz}^{elastelect} + U_{pz}^{elect} \quad (3)$$

where  $U_{pz}^{elast}$  is the elastic energy stored due to the elasticity of the material,  $U_{pz}^{elastelect}$  represents the further elastic energy due to the voltage driven piezoelectric effect, and  $U_{pz}^{elect}$  is the electric energy stored due to the dielectric rigidity of the piezoelectric material and

$$\begin{aligned}
U_{pz}^{\text{elast}} &= \frac{1}{2} \boldsymbol{\phi}^t \mathbf{K}_{pz}^{\text{elast}} \boldsymbol{\phi} \\
U_{pz}^{\text{elastelect}} &= \mathbf{v}^t \mathbf{K}_{pz}^{\text{elastelect}} \boldsymbol{\phi} \\
U_{pz}^{\text{elect}} &= \frac{1}{2} \mathbf{v}^t \mathbf{K}_{pz}^{\text{elect}} \mathbf{v}
\end{aligned} \tag{4}$$

where  $\mathbf{v}$  denotes the vector of the voltages at the piezoelectric patches. Then, when all the energy expressions are available, application of Lagrange's equations of motion, i.e.

$$\frac{d}{dt} \left( \frac{\partial T}{\partial \dot{q}_i} \right) - \frac{\partial T}{\partial q_i} + \frac{\partial U}{\partial q_i} = Q_i \tag{5}$$

where:

$$T = T_{pl} + T_{pz} \quad U = U_{pl} + U_{pz} \tag{6}$$

and  $Q_i$  are the generalised forces and  $q_i$  the generalised co-ordinates, becomes quite straight forward and yields:

$$\left( \mathbf{M}_{pl} + \mathbf{M}_{pz} \right) \ddot{\boldsymbol{\phi}} + \left( \mathbf{K}_{pl} + \mathbf{K}_{pz}^{\text{elast}} \right) \boldsymbol{\phi} + \left( \mathbf{K}_{pz}^{\text{elastelect}} \right)^t \mathbf{v} = \mathbf{Q} \quad \mathbf{K}_{pz}^{\text{elastelect}} \boldsymbol{\phi} + \mathbf{K}_{pz}^{\text{elect}} \mathbf{v} = 0 \tag{7}$$

The first equation here describes the dynamics of the system when the piezoelectric patches are used as actuators (externally driven) and can be rewritten as

$$\mathbf{M}_{acp} \ddot{\boldsymbol{\phi}} + \mathbf{C}_{acp} \dot{\boldsymbol{\phi}} + \mathbf{K}_{acp} \boldsymbol{\phi} = \mathbf{V}_a \mathbf{v}_a + \mathbf{S}_f \mathbf{f} \tag{8}$$

where  $\mathbf{f}$  is the vector constructed from the external forces.

The second equation in (7) can be rewritten as:

$$\mathbf{v}_s = - \left( \mathbf{K}_s^{\text{elect}} \right)^{-1} \mathbf{K}_s^{\text{elastelect}} \boldsymbol{\phi} \tag{9}$$

and used to retrieve the voltages at the patches acting as sensors.

In control systems terms, the model derived above is a multiple-input multiple-output (MIMO) linear system. Also the inputs and outputs each split into two groups. In

particular, the inputs consist of the elements of the disturbance vector  $\mathbf{f}$ , which cannot be monitored, and the elements in the vector  $\mathbf{v}_a$ , which are the voltages which will be applied to the actuators by the control system output vector.

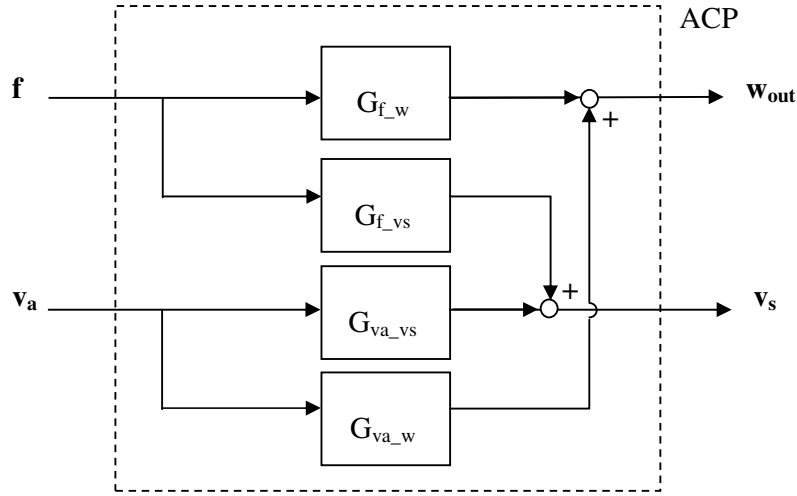


**Figure 3: ACP input/output block diagram structure**

The outputs consist of the elements in the vector  $\mathbf{v}_s$  as measured by the sensors, and the displacements  $\mathbf{w}_{out}$  at certain locations on the panel which cannot be directly measured. Figure 3 shows a schematic diagram of the structure of the plant in this context. In this general application area, the actuators and sensors will often be non co-located. This, in turn, means that non-minimum phase behaviour is highly likely to occur in the underlying plant dynamics (with immediate implications in terms of control). To illustrate this point consider, for simplicity, the transfer function  $G_{va\_vs}(s)$  between  $v_a$  and  $v_s$  in the single-input single-output case, i.e.

$$G_{va\_vs}(s) = \frac{v_s(s)}{v_a(s)} = -(\mathbf{K}_s^{elect})^{-1} \mathbf{K}_s^{elastolect} (\mathbf{M}_{acp} s^2 + \mathbf{C}_{acp} s + \mathbf{K}_{acp})^{-1} \mathbf{V}_a \quad (10)$$

whose pole zero plot is shown in Figure 4a, thus confirming the presence of non-minimum phase dynamics.

The other transfer functions in this particular case are

$$G_{f_w}(s) = \frac{W_{out}(s)}{f(s)} = \mathbf{C}_w (\mathbf{M}_{acp} s^2 + \mathbf{C}_{acp} s + \mathbf{K}_{acp})^{-1} \mathbf{S}_f \quad (11)$$

and

$$G_{va_w}(s) = \frac{W_{out}(s)}{V_a(s)} = \mathbf{C}_w (\mathbf{M}_{acp} s^2 + \mathbf{C}_{acp} s + \mathbf{K}_{acp})^{-1} \mathbf{V}_a \quad (12)$$

respectively, each of which has a pole-zero cancellation of the 7<sup>th</sup> mode, as illustrated in Figure 4b for the case of  $G_{f_w}(s)$ . In physical terms this means that the point where the displacement is evaluated is on a nodal line of the 7<sup>th</sup> mode, as highlighted in Figure 5.

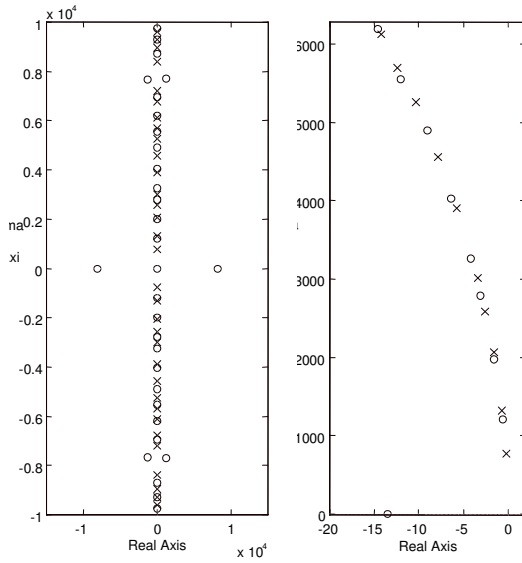


**Figure 4a: Pole zero pattern for the transfer function  $G_{va_vs}(s)$**

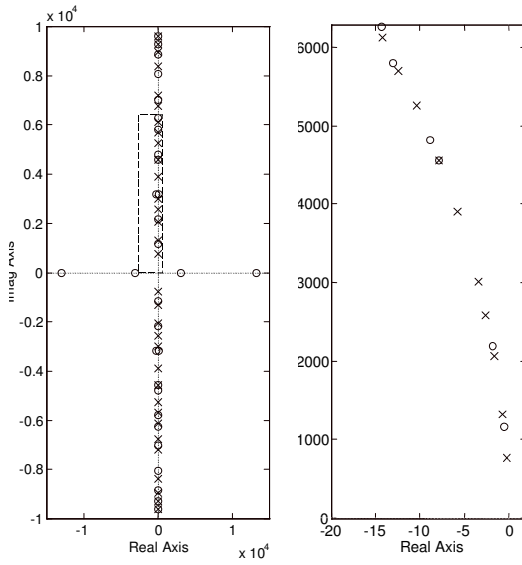


**Figure 4b: Pole zero pattern for the transfer function  $G_{L_w}(s)$ .**

Controller design can be undertaken in either the state space or transfer function domains. In particular, the underlying mathematical model can be immediately written in the required form for either design methodology. In the remainder of this paper,  $H_\infty$  based active feedback control schemes for disturbance attenuation are designed.

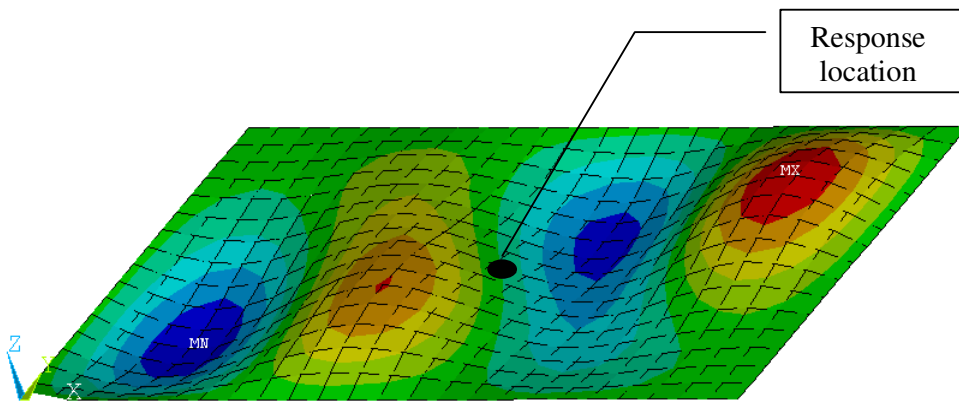


**Figure 5: 7<sup>th</sup> mode of the ACP with response location**

## H<sub>∞</sub> CONTROLLER DESIGN

The state space model of the previous section can be immediately expressed in the standard H<sub>∞</sub> problem setting and, in particular, the so-called 4-block form. In this case since the control signals and disturbances are physically different and applied at different locations, they influence the dynamics in rather different ways. Similarly the two groups of outputs are rather different and, due to the impossibility of directly measuring the first group of outputs, these have to be appropriately inferred from the second group. The basic physical objective of a control scheme in this problem area is to eliminate, or at least substantially reduce, the resonance peaks in the frequency response of the plant to the input disturbances.

It will be demonstrated below that this 'flattening down' of the response can be achieved by an un-weighted H<sub>∞</sub> sensitivity design. The model here is already in a 4 block form, which is the typical format used for an H<sub>∞</sub> controller to be applied, but the software available for H<sub>∞</sub> design requires a regularisation of the model description. In its original form, the plant here has state space realisation defined by

$$\left[ \begin{array}{c|cc} \mathbf{A} & \mathbf{B}_f & \mathbf{B}_v \\ \hline \mathbf{C}_w & \mathbf{D}_{11} & \mathbf{D}_{12} \\ \mathbf{C}_v & \mathbf{D}_{21} & \mathbf{D}_{22} \end{array} \right] \quad (13)$$

where  $\mathbf{D}_{11}$ ,  $\mathbf{D}_{12}$ ,  $\mathbf{D}_{21}$  and  $\mathbf{D}_{22}$  are zero matrices of appropriate dimensions, but this is not allowed by the H<sub>∞</sub> software, which requires:

$$\text{rank}(\mathbf{D}_{12}) = \dim(v_a) \leq \dim(w_{out}) \quad (14a)$$

$$\text{rank}(\mathbf{D}_{21}) = \dim(v_s) \leq \dim(f) \quad (14b)$$

The procedure used to produce a direct feed-through between control input and inferred outputs and between disturbances and measurements, which is implicit in (14a) and (14b), is termed regularisation. In principle this problem could be solved by assuming  $\mathbf{D}_{21} = \epsilon_1 \mathbf{v}$  and  $\mathbf{D}_{12} = \epsilon_2 \mathbf{f}$  with  $\epsilon_1$  and  $\epsilon_2$  as small as possible. However, this would mean that the new system response is given by:

$$\begin{aligned}\mathbf{w}_{\text{out}} &= \mathbf{C}_w \mathbf{x} + \varepsilon_1 \mathbf{v}_a \\ \mathbf{v}_s &= \mathbf{C}_v \mathbf{x} + \varepsilon_2 \mathbf{f}\end{aligned}\tag{15}$$

and the selection of  $\varepsilon_1$  and  $\varepsilon_2$  large enough to satisfy the  $H_\infty$  software would drastically change the zero structure of the plant and hence give useless results.

A better way to regularise the system is through an appropriate augmentation procedure where some fictitious disturbances  $\boldsymbol{\varphi}$  and some fictitious controlled outputs  $\boldsymbol{\delta}$  are added to the original system. The augmented plant will therefore have a disturbance input vector and a vector of the controller variables given by:

$$\mathbf{u}_1 = \begin{pmatrix} \mathbf{f} \\ \boldsymbol{\varphi} \end{pmatrix} \text{ and } \mathbf{y}_1 = \begin{pmatrix} \mathbf{w} \\ \boldsymbol{\delta} \end{pmatrix}\tag{16}$$

and a state space realisation:

$$\left[ \begin{array}{ccc|c} \mathbf{A} & \mathbf{B}_f & 0 & \mathbf{B}_v \\ \mathbf{C}_w & 0 & 0 & 0 \\ 0 & 0 & 0 & \varepsilon_1 \mathbf{I} \\ \hline \mathbf{C}_v & 0 & \varepsilon_2 \mathbf{I} & 0 \end{array} \right]\tag{17}$$

which can be represented by the block diagram of Figure 6.

The two parameters  $\varepsilon_1$  and  $\varepsilon_2$  produce the direct feed-through required by the  $H_\infty$  software. The first parameter  $\varepsilon_1$  can be interpreted as a penalty function on the control signal, a large value of  $\varepsilon_1$  produces a relatively small control input. Conversely, reducing  $\varepsilon_1$  it is possible to increase the control action. The second parameter,  $\varepsilon_2$ , can be interpreted as a disturbance, such as noise, injected on the sensed output. Selecting a large value for  $\varepsilon_2$  means very limited trust in the sensor's measurements and the result will be a relatively low observer gain. Conversely, a small value of  $\varepsilon_2$  produces much larger observer gains.

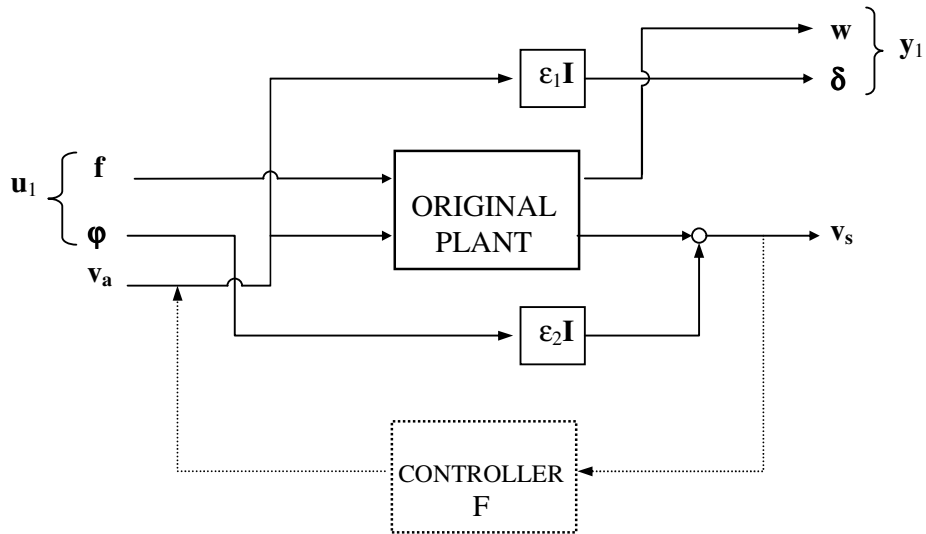


**Figure 6: Augmented system block diagram**

Comparing the augmented system with the original one it is seen that norm of the transfer function between  $\mathbf{u}_1$  and  $\mathbf{y}_1$  is greater than or equal to the norm of the transfer function from  $\mathbf{f}$  to  $\mathbf{w}$ . Furthermore by letting  $\epsilon_1$  and  $\epsilon_2$  tend to zero the norm for the transfer function for the augmented system tends to that one of the original system. Consequently, a controller designed for the augmented system will work also for the original system. This problem setup is considered in detail next.

Recall that the physical objective of this design problem is to eliminate, or at least substantially reduce, the resonant peaks in the frequency response of the plant in response to input disturbances. It is easy to see that in this set-up the closed loop transfer function from  $\mathbf{f}$  to  $\mathbf{w}_{\text{out}}$  in (15) has a  $H_\infty$  norm less than or equal to the  $H_\infty$  norm of the closed loop transfer function from  $\mathbf{u}_1$  to  $\mathbf{y}_1$  in the system in (16) - (17). Also as  $\epsilon_{1,2} \rightarrow 0$  the latter  $H_\infty$  norm tends to the former for the central controller. Hence designing a controller for the latter system will yield a controller that gives 'high performance' when applied to the original system.

The actual selection of  $\epsilon_1$  and  $\epsilon_2$  is an iterative procedure where, intuitively  $\epsilon_1$  relates to the feedback problem whereas  $\epsilon_2$  relates to the estimation problem. Although the separation property of  $H_\infty$  theory is much more complicated than the similar property for  $H_2$  theory, in actual practice the selection of the two parameters can be done quite independently.

Hence, reasonable values of  $\epsilon_1$  and  $\epsilon_2$  can be obtained by two (convex) line searches. First  $\epsilon_1$  is found by, for example, a bisection procedure to yield a value of the closed loop  $H_\infty$  norm  $\|\mathbf{G}_{f-w}(s)\|_\infty$  which is sufficiently small, whilst keeping the controller gains reasonably bounded. This procedure is then repeated for  $\epsilon_2$ . This flattening down of the response can therefore be achieved by an un-weighted  $H_\infty$  sensitivity design which, by minimising the transfer function norm (i.e. minimising the sensitivity), should achieve the desired disturbance rejection.

Consider again the particular case of Figure 1, with the dimensions and material properties given in Table 1. Then by following the above design process,  $\epsilon_1 = 1.99 \cdot 10^{-8}$  and  $\epsilon_2 = 10^{-3}$  have been selected. Figure 7 shows the frequency response of the resulting open and closed loop transfer functions. These are the for the response at the centre of the panel to a sinusoidal disturbance force of amplitude 1 Newton, applied at another point on the panel.

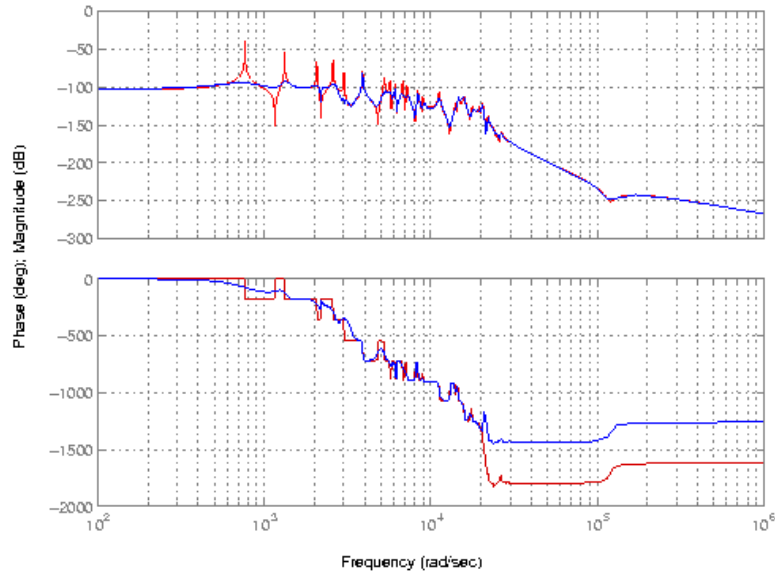


**Figure 7: Bode diagram for the open-loop and closed-loop plant.**

This shows that almost all of the resonant peaks (in the range of interest) are significantly reduced - for the first mode this is up to 60 dB (Note the wide range logarithmic scale used.) However (and surprisingly) even most of the peaks below DC - performance are also significantly reduced. This is not an inherent property of  $H_\infty$

controllers. In fact, sometimes the 'flattening' property of  $H_\infty$  control can result in worse closed loop behaviour over some frequency ranges.

Fortunately though, for the actual case, the computed central  $H_\infty$  controller achieves closed loop disturbance attenuation in all relevant frequency regions, in spite of the fact that a completely un-weighted design was made. Hence there is no need to introduce a narrow band-pass dynamic weights for the optimisation problem which could cause numerical and/or robustness problems.

Figure 8 shows another representation of the closed loop frequency response. Note that the  $H_\infty$  controller is able to significantly reduce all the resonance peaks including the resonance peak at 620 Hz. The deformed shapes of the vibrating panel with and without control respectively are shown in Figure 9. It is surprising that these results are produced without increasing the voltage (Figure 10) which drives the actuator. In physical terms it is clear that  $H_\infty$  control is capable of modifying the deformed shape of the panel, shown in Figure 11 so to avoid the problem of the flexural line running half way through the actuator.

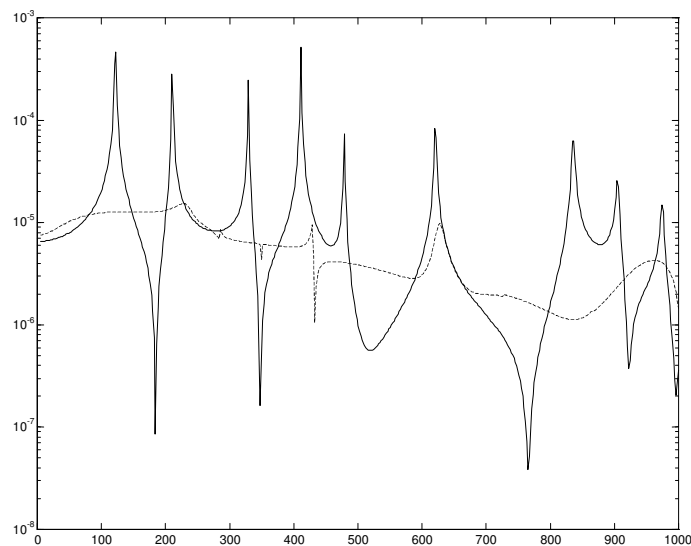


**Figure 8: Frequency response at the centre of the panel with (dashed line) and without (continuous line)  $H_\infty$  controller.**

## CONCLUSIONS

This paper has described the design of  $H_\infty$  based active feedback control schemes for the suppression of microvibrations on a mass loaded panel. The model used in the design has been developed using a Lagrange Rayleigh Ritz modelling procedure

developed previously [1]. It is clear that this approach is capable of producing high quality implementable designs. It is important to note, however, that the designs given here are for sensitivity minimisation (i.e. disturbance rejection) only. An obvious next step is to undertake robust controller design studies for which it will be necessary to obtain a parameterisation of the uncertainties present. Some first ideas on how this could be achieved can be found in [2].

There is much work still to be done in this general area, both for actively controlled panels and the more general case of equipment loaded panels. Some basic ideas and first results in this context can also be found in [2].

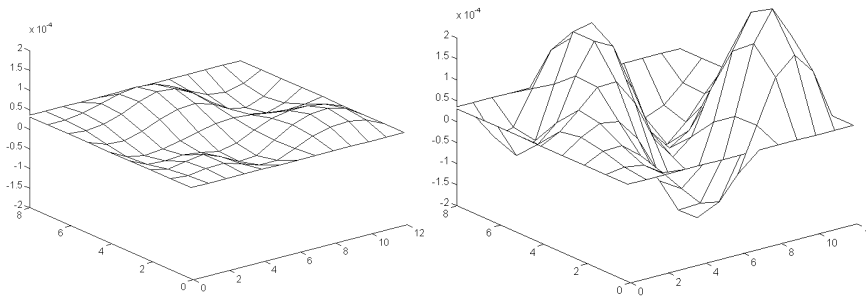


**Figure 9: Deformed shapes of the panel at 620Hz, with and without control respectively**

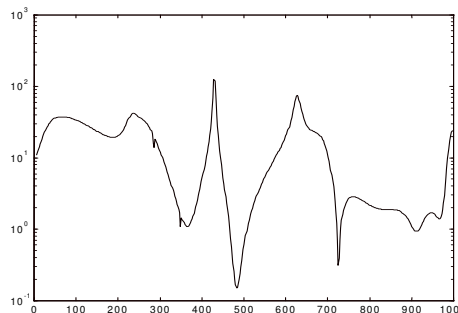


**Figure 10: Voltage signal driving the actuator**

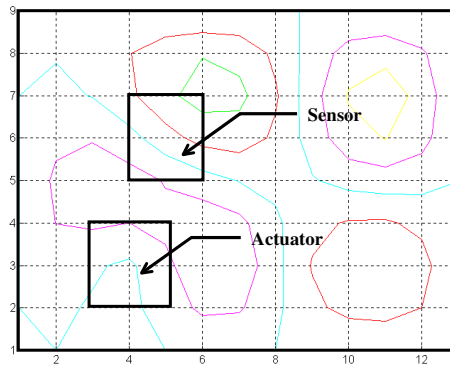


Figure 11: Contour plot at 620 Hz

**Dimensions**

<b>plate</b>		
a		304.8 mm
b		203.2 mm
h		1.524 mm
<b>sensor</b>		
xs <sub>1</sub>		50.8 mm
xs <sub>2</sub>		101.6 mm
ys <sub>1</sub>		25.5 mm
ys <sub>2</sub>		76.2 mm
hpzs		191 10 <sup>-3</sup> mm
<b>Actuator</b>		
xa <sub>1</sub>		76.2 mm
xa <sub>2</sub>		127 mm
ya <sub>1</sub>		101.6 mm
ya <sub>2</sub>		152.4 mm
hpza		191 10 <sup>-3</sup> mm
<b>lumped mass</b>		
xlm		50.8 mm
ylm		152.4 mm

**Material properties**

<b>plate</b>		
E		71 10 <sup>9</sup> Pa
ρ		2800 kg/mm <sup>3</sup>
ν		0.33
<b>sensor</b>		
E		63 10 <sup>9</sup> Pa
ρ		7650 kg/mm <sup>3</sup>
ν		0.3
d		1.66 10 <sup>-10</sup> m/volt
<b>actuator</b>		
E		63 10 <sup>9</sup> Pa
ρ		7650 kg/mm <sup>3</sup>
ν		0.3
d		1.66 10 <sup>-10</sup> m/volt
<b>lumped mass</b>		
Wlm		0.05 kg

Table 1: Actively controlled panel data

**REFERENCES:**

[1] G.S.Aglietti, S.B.Gabriel, R.S.Langley and E.Rogers, 'A Modelling Technique For Active Control Design Studies With Application To Spacecraft Microvibrations', Journal of The Acoustical Society of America, 102 (4) pp. 2158-2166, October 1997.

[1] G.S. Aglietti, Active Control of Microvibrations for Equipment Loaded Spacecraft Panels, PhD Thesis, University of Southampton, UK, 1999.